

# Self-Sensing versus Reference Air Gaps

Alexander Schulz, Ingrid Rottensteiner, Manfred Neumann, Michael Wehse, Johann Wassermann

**Abstract**—Self-sensing estimates the air gap within an electro magnetic path by analyzing the bearing coil current and/or voltage waveform. The self-sensing concept presented in this paper has been developed within the research project “Active Magnetic Bearings with Supreme Reliability” and is used for position sensor fault detection.

Within this new concept gap calculation is carried out by an all-digital analysis of the digitized coil current and voltage waveform. For analysis those time periods within the PWM period are used, which give the best results. Additionally, the concept allows the digital compensation of nonlinearities, for example magnetic saturation, without degrading signal quality. This increases the accuracy and robustness of the air gap estimation and additionally reduces phase delays.

Beneath an overview about the developed concept first measurement results are presented which show the potential of this all-digital self-sensing concept.

**Keywords**—digital signal analysis, active magnetic bearing, reliability, fault detection.

## I. INTRODUCTION AND STATE OF THE ART

TYPICALLY, self-sensing is used to eliminate the requirement for position sensors within active magnetic bearings (AMBs) by estimating the position of the levitated object from measuring and analyzing the bearing coil current and/or voltage waveform. Benefits of this technique are:

- Lower initial system costs,
- reduced bearing size, as no space for mounting the discrete position sensors is required,
- co-location of magnetic actuator and sensor, thus reducing active magnetic bearing controller complexity.

The self-sensing concept presented in this paper is used for position sensor fault detection and is one of the key elements

within the nationally supported research project “Active Magnetic Bearings with Supreme Reliability” (see [9] - [14]).

A. Schulz is with the Institute of Mechanics and Mechatronics, Vienna University of technology, 1040 Vienna, Austria (e-mail: alexander.schulz@tuwien.ac.at).

I. Rottensteiner was with Vienna University of technology. She is now with Test-Fuchs (i.rottensteiner@test-fuchs.com).

M. Neumann is with the Institute of Mechanics and Mechatronics, Vienna University of technology, 1040 Vienna, Austria (e-mail: manfred.neumann@tuwien.ac.at).

M. Wehse is with the Institute of Mechanics and Mechatronics, Vienna University of technology, 1040 Vienna, Austria (e-mail: michael.wehse@tuwien.ac.at).

J. Wassermann is with the Institute of Mechanics and Mechatronics, Vienna University of technology, 1040 Vienna, Austria (e-mail: johann.wassermann@tuwien.ac.at).

Within this research project a comprehensive concept for active magnetic bearings’ reliability has been developed, which offers supreme reliability of the whole system over the whole operating time, whereby bearing capacity is maintained even in case of a defect within any sub-assembly.

Currently, there are two different approaches for self-sensing AMBs. The first approach treats the magnetic bearing and the supported object as a whole system, thus considering the position as a state. The second approach is based on measuring the change of inductance caused by rotor displacement.

The state estimation method, introduced in [18], is based on the model of the AMB-system. Position is estimated by using a linear state estimator as observer. Reference [3] explains, that AMB system stability using state estimation method can only be achieved at the expense of system robustness.

Since the gap displacement modulates the amplitude of the switching amplifier output waveform, the Fourier coefficients of the voltage and current signals at the switching frequency are used for position estimation in [7]. Because the estimation result not solely depends on gap displacement but also on the duty-cycle of the PWM switching amplifier (force feed-through), a nonlinear compensator for the duty cycle is suggested. A self-sensing method using test-signal injection, whose basis is derived from sensorless reluctance motors, is stated in [1].

A combination of test-signal injection and direct detection is presented in [2]. For inductance measurement at low frequencies a signal above audible range is induced and its amplitude is detected. Higher frequency variation of inductance is detected from voltage and current signals. These two combine to give a measure of the gap and the rate of change of gap. To cope with nonlinearities due to saturation in the magnetic core the current through the opposite - unsaturated - electro magnet is used.

In [6] a nonlinear parameter estimation technique is presented. A rather complex all-analog signal processing filter demodulates the switching waveform of bi-state switching amplifiers which drive the coils. The rejection of force feed-through (duty cycle change) is achieved by adding a parallel simulation of an inductor model, whose output passes through the same filter as the actual current waveform. The error between actual and simulated inductance is used to correct the model. In [5] simulation results and hardware implementation for an AMB test rig are presented.

Reference [4] presents a feedback control for active magnetic bearings based on current change rate alone. Switching amplifier input and output terminals and the magnet

coils are connected to a network composed of a transformer and a sample-and-hold circuit. When sampling takes place at a certain moment of each PWM cycle, the electronics give a full state feedback that can stabilize the rotor.

In [8] position estimation considers the first harmonic of the voltage and current waveforms. They are obtained by using a band-pass filter and demodulation, resulting in that all signals have the rather low mechanical frequency bandwidth. The inverse permeability is approximated by a polynomial of second order representing the unhysteretic B-H characteristic. The realized position estimation hardware for a test rig consists of all-analog band-pass filters and demodulation. Influences by the voltage duty-cycle as well as the magnetic saturation are compensated within a digital signal processor (DSP).

Generally, it is stated in [5] and [8] that all methods for self-sensing, presented so far are very delicate to realize, lack robustness, and none has shown acceptable performance for industrial application on a levitated rotor. One major reason is the all-analog implementation within almost all cases (exceptions are e.g. in [8] and [17]), resulting in very complex electronic circuitry if a certain level of accuracy shall be achieved, which states the following problems:

- Sensitivity to electrical noise, electromagnetic interference, component tolerances, aging, etc.,
- phase shifts due to the number of filters,
- compensation of magnetic nonlinearities is difficult and amplifies the above stated problems.

## II. AN ALL-DIGITAL SELF-SENSING CONCEPT

### A. Overview

The developed all-digital self-sensing concept belongs to the group of self-sensing approaches which directly uses the PWM-output voltage of the switching amplifier as high frequency “test signal” source. The air gap is calculated without the need for demodulation, high order filtering, etc. It is directly based on the estimation of inductance, which is mainly a function of the air gap of the electro magnet but also a function of the coil current and the driving voltages’ frequency content, too.

In contrary to all concepts known from literature, here, air gap calculation is carried out by direct online analysis of the coil current waveform and the coil driving voltage waveform.

The block diagram of an advantageous embodiment is shown in Fig. 1. A direct digitally controlled power switching amplifier drives an electro magnet. The coil driving signals are digitized with a high sampling rate (at least 10 times the PWM frequency) and analyzed using the information about the exact switching times and characteristics of the power amplifier and measurement signal chain. For analysis those time periods within the PWM period are used, which give the best results.

Here, the coil voltage is calculated based on the amplifiers’ link voltage, the actual switching state and the known voltage losses of the switching elements (power transistors and free-wheeling diodes) as well as the ohmic losses (printed circuit board, connectors, cabling and the coil). Calculating the coil voltage this way allows cheaper voltage sensors with highly reduced upper frequency limit compared to direct measurement of the amplifier output voltage.

As single disturbances have only a rather low impact on the final result due to the high sampling rate, a by fare higher robustness against electromagnetic interferences can be gained compared with all concepts known from literature, where for example band-pass sampling with a low digitization sampling rate is used, as for example in [8].

The self-sensing algorithm can be implemented within a fast micro controller ( $\mu\text{C}$ ), a DSP or a field programmable gate array (FPGA). Depending on available processing power, this allows flexibility in signal analysis, and additionally, the digital compensation of nonlinearities, for example magnetic saturation (see [8], e.g.), without degrading signal quality. This increases the accuracy and robustness of the air gap estimation and additionally reduces phase delays. Details on the principle and advantages of this new concept, as well as simulation results, will be presented in [15].

An effective and easy-to-implement method is used to show the basic principle of the self-sensing concept presented within this paper: During the known time slot, where the amplifier PWM control signals cause a significant positive or negative coil current slope, the coil current slope is calculated, and by additionally analyzing the switching amplifier link voltage and considering magnetic saturation, the position is estimated.

An example for a much more sophisticated method is the use of an observer to minimize the difference between the actual current waveform and a simulation including the detailed model of the mechanic, magnetic, and electric system.

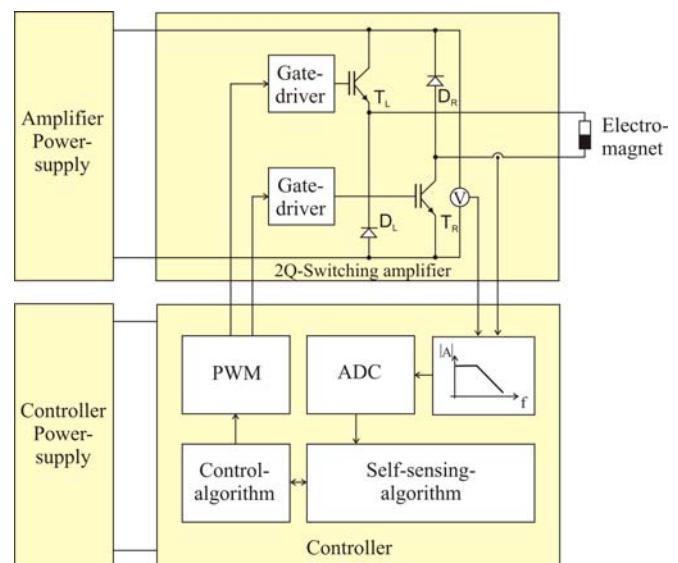


Fig. 1 Hardware block diagram of the all-digital self-sensing concept

### B. Air gap calculation

As for all test signal based self-sensing approaches, the dynamics of the mechanic system are neglected over the electric system. This means, that the air gap is assumed to be constant during one PWM period. Additionally, stray flux within the electro magnet is neglected (see Fig. 2), and the relative permeability of the iron is assumed to be constant during one PWM period.

Fig. 3 shows the schematic control signals for the power amplifier switching transistors of one PWM period with positive amplifier output voltage, followed by one PWM period with negative amplifier output voltage as well as the schematic resulting voltage and current waveforms including switching delays and switching induced oscillations on the coil current sensor signal.

As the derivation of the equations for calculating the air gap is carried out in detail in [15], within this paper only a summary of the main equations used for air gap calculation is given.

In the first calculation step the mean current gradient  $\overline{dI(n)}/dt$  of the current PWM period  $n$  is calculated during the time where both PWM-transistor control signals are logical high or low by averaging the available current gradients  $k1$  to  $k2$  at sample number  $i$  (see Fig. 3) using central difference quotients, whereby  $t_s$  is the sampling interval and all sampling values with switching induced transient effects (du/dt-induced oscillations within the current sensor signal, etc.) are excluded from the calculation.

$$\frac{dI(i)}{dt} = \frac{I(i+1) - I(i-1)}{2 \cdot t_s} \quad (1)$$

$$\overline{\frac{dI(n)}{dt}} = \frac{1}{1 + k2 - k1} \sum_{i=k1}^{k2} \frac{dI(i)}{dt} \quad (2)$$

In the second step, the arithmetic mean value of all samples during the time where the coil current is almost constant (exactly one of the PWM transistor control signals is high),  $I_{PW}$  is calculated.

In the third step the inductance  $L_{EM}$  of the electro magnet shown in Fig. 2 is calculated using faraday's law of induction and Kirchhoff's voltage law.

$$L_{EM} = \frac{U_{LV} - \text{sign}\left(\frac{dI(n)}{dt}\right) \left( R_{ohm\Sigma} I_{PW} - U_{Loss\Sigma} \cdot \text{sign}\left(\frac{dI(n)}{dt}\right) \right)}{\left| \frac{dI(n)}{dt} \right|} \quad (3)$$

With the amplifier link voltage  $U_{LV}$ , the sum of the ohmic resistances (inductance, cabling, and connectors)  $R_{ohm\Sigma}$ , and the sum of all voltage losses from switching elements  $U_{Loss\Sigma}$ . Depending on the switching state (both transistors or both

free-wheeling diodes are in conducting state),  $U_{Loss\Sigma}$  has different values.

In a fourth step the flux densities of the rotor and stator iron,  $B_R$  and  $B_S$ , are evaluated using the cross section area of the rotor iron  $A_{EM\_R}$ , and the cross section area of the stator iron  $A_{EM\_S}$ , as well as the coil winding number  $N_{EM}$ . The additional multiplier two in the nominator of (4) results from flux splitting in the E-core which can be seen in Fig. 2.

$$B_R = \frac{L_{EM} \cdot I_{PW}}{2 \cdot A_{EM\_R} \cdot N_{EM}} \quad (4)$$

$$B_S = \frac{L_{EM} \cdot I_{PW}}{A_{EM\_S} \cdot N_{EM}} \quad (5)$$

With the flux densities the relative permeability of the rotor and stator iron (magnetic nonlinearity),  $\mu_{rR}$  and  $\mu_{rS}$ , is calculated as in [14], using the approximated unhysteretic magnetization curve (see Fig. 4). To get the relative permeability, the unhysteretic magnetization curve is differentiated with respect to the magnetic field  $H$  and divided by the permeability of vacuum  $\mu_0$ . The unhysteretic magnetization curve in Fig. 4 is approximated by averaging the left hand and right hand magnetization path of a measured B-H-magnetization curve.

In the last step the air gap  $s_g$  is calculated using the magnetic resistance of the electro magnetic path  $\mathfrak{R}_{EM}$ , the flux path length within the stator and rotor iron,  $l_{EM\_S}$  and  $l_{EM\_R}$ , and the inductance  $L_{EM}$ .

$$\begin{aligned} \mathfrak{R}_{EM} &= \frac{1}{\mu_0} \left( \frac{l_{EM\_S}}{A_{EM\_S} \cdot \mu_{rS}} + \frac{l_{EM\_R}}{2 A_{EM\_R} \cdot \mu_{rR}} + \frac{2s_g}{A_{EM\_S}} \right) = \\ &= \frac{N_{EM}^2}{L_{EM}} \end{aligned} \quad (6)$$

$$s_g = \frac{N_{EM}^2 \mu_0 \cdot A_{EM\_S}}{2L_{EM}} - \frac{l_{EM\_S}}{2\mu_{rS}} - \frac{l_{EM\_R} \cdot A_{EM\_S}}{4A_{EM\_R} \cdot \mu_{rR}} \quad (7)$$

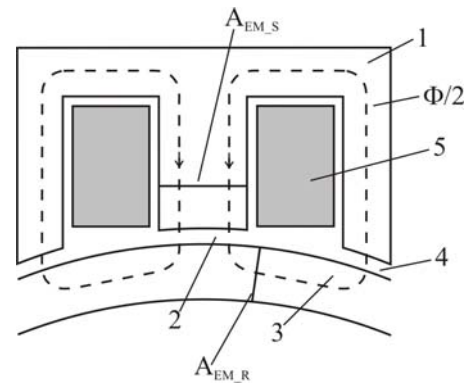


Fig. 2: Electro magnet: (1) stator iron core (E-core), (2) and (4) air gap, (3) rotor iron core, (5) coil winding, ( $\Phi$ ) magnetic flux, ( $A_{EM\_R}$ ) cross section area of the rotor iron, and ( $A_{EM\_S}$ ) cross section area of the stator iron

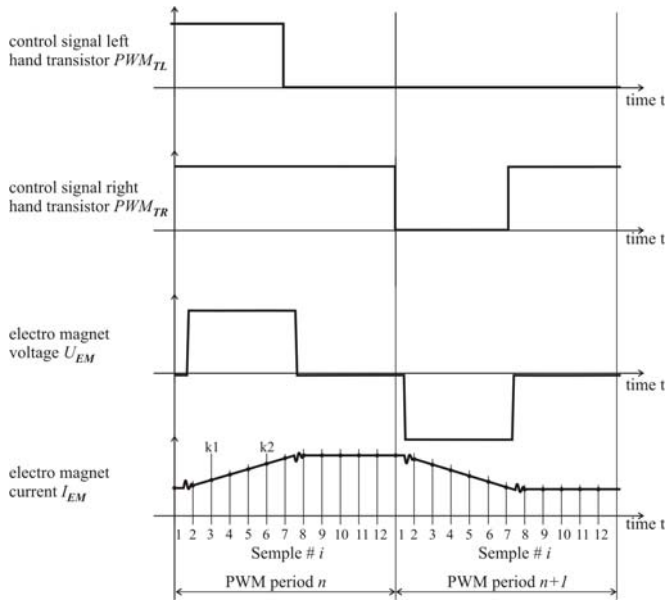


Fig. 3 PWM-signals and resulting electromagnet voltage and current waveforms (schematic)

### III. EXPERIMENTAL RESULTS

To test the basics of the proposed self-sensing concept a PC-controlled test stand has been constructed (see Fig. 5). It allows automated measurement of electro magnet characteristics, namely force, current, and displacement. The test electro magnet has been driven using a specially hot swap controller amplifier module developed for the active magnetic bearing with supreme reliability (see Fig. 6, and [12], e.g.). This hot swap controller amplifier module comprises two digital signal controllers, a switching amplifier, local power supplies, and a local error detection unit. The digital bearing controller is implemented within digital signal controller one and the implementation of the error detection is split into both digital signal controllers. Whereby, all-digital self-sensing will be carried out in the second digital signal controller.

The bearing controller within the hot swap controller amplifier module has been programmed as current controller with a reference current profile which can be seen in Fig. 10. The reference current is increased stepwise from  $I_{PW} = 1$  A to  $I_{PW} = 25$  A, whereby in each step the first three PWM periods are used to reach the reference current and the fourth PWM period is used to set a constant pulse width. After reaching the maximum current the reference current is decreased to the minimum current value using the same scheme as before. This test cycle is repeated for three different constant pulse widths, namely 33 %, 50 % and 67 %.

All in all, the results of five of these current sequences have been analyzed for exemplary reference air gaps  $s_{g\_REF}$  of 0.65 mm, and 0.5 mm within this paper.

To test the basic functionality (almost) without the influence of sensor transfer behavior, the following measurement results have been carried out using a reference current probe A6303 and TM502A as well as a reference differential probe P5205 from Tektronix. The signals have

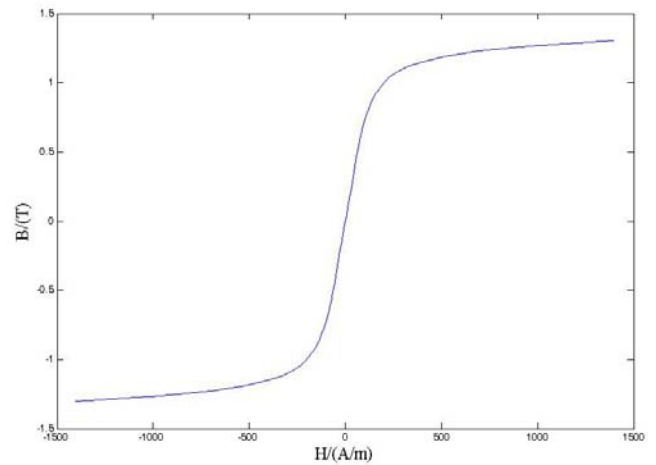


Fig. 4 Approximation of the unhyseretic magnetization curve of soft magnetic iron M111-35N (calculated through averaging the left hand and right hand path of a measured B-H-magnetization curve)

been captured using a mixed signal oscilloscope TMO4034 from Tektronix with a sampling rate of 2.5 GSamples/s, internally averaged and down-sampled to 10 MSamples/s (recording depth: 100 kSamples) and transferred to a PC. The self-sensing algorithm is executed on the PC using Matlab.

First, measurement data are low pass filtered using a first order filter with a cut-off frequency of 1.6 MHz. The resulting voltage and current waveforms of one complete measurement sequence can be seen in Fig. 7 and Fig. 10. The voltage and current signals of one PMW period with positive output voltage and one PWM period with negative output voltage can be seen in Fig. 8 and Fig. 9, and Fig. 11 and Fig. 12 respectively. It can be seen in Fig. 9 and 12 that the shape of the current ripple waveform is not the expected clean almost linear increasing/decreasing current slope during significant amplifier voltages as well as the almost constant current value during the almost zero amplifier output voltage. The cusps in the current waveforms that appear at each switching instant are caused almost entirely by eddy current in the soft magnetic iron of stator and rotor (see [16]). These eddy current caused differences between expected and existent current waveforms are one reason why previous self-sensing concepts did not perform very well in many cases. Using the self-sensing concept presented within this paper, the sample values showing eddy current influences can simply be excluded from air gap calculation.

In a next step, the offset voltage and the ohmic resistance of the electro magnet coil  $R_{ohmEM}$  is calculated and the offset voltage is compensated. Then, the starting time value of each PWM period is detected within the voltage signal, and averaging and down sampling to 12 sample values per PWM period of the current signal is carried out. This is done, to test

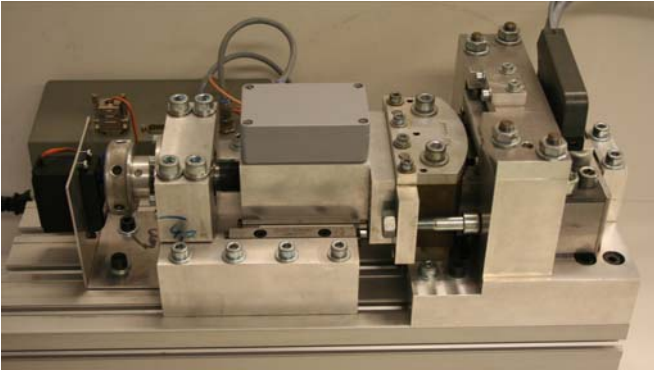


Fig. 5 PC-controlled self-sensing test stand



Fig. 6. Insight into a hot swap controller amplifier module prototype: digital signal controller section with digital signal control-cards (Texas Instruments TMS320F28335) on the lower side; power stage with 25 kVA in the centre and low level power supply transformers (400Vac to 230Vac) and mains switch on the upper side.

achievable signal quality under the same conditions as within the first application - the active magnetic bearing with supreme reliability, where four-times oversampling and averaging is used, which is the maximum the used  $\mu\text{C}$  can analyze online, as the  $\mu\text{C}$  has to carry out other tasks, additionally. Further on, inductance is calculated using (3), but as the amplifier output voltage is measured directly in this test setup,  $U_{Loss\Sigma}$  is zero and  $R_{ohm\Sigma}$  is only the ohmic resistance of the electro magnet coil  $R_{ohmEM}$ .

The air gap is calculated using (7) whereby the relative permeability is calculated according to chapter II using (4) and (5) combined with a  $\mu_o$ -B look-up table. To further improve the calculation results, a current depending compensation has been used which leads to the results shown in Fig. 13 to Fig. 18.

As all coil current samples which reduce analysis' accuracy due to amplifier switching or eddy currents are excluded from coil current slope analysis, and there are only 12 sample values per full PWM period available within the first hardware-implementation, only pulse widths over 45 % can be analyzed satisfactorily.

The self-sensing results for a reference air gap of 0.65 mm (see Fig. 13 – Fig. 15) and 0.5 mm (see Fig. 16 – Fig. 18) show very good results with a narrow peak in the histogram of Fig. 14 for  $s_{g\_REF} = 0.65$  mm and also a good result with a little bit broader peak for  $s_{g\_REF} = 0.5$  mm in Fig. 17. In Fig. 16 the reason for this broader peak can be seen: There is a slight tendency of the algorithm to calculate smaller air gap values when coil current is over 18 A despite using the said current compensation.

With further decreasing air gaps the peak broadens as the assumption of constant magnetic nonlinearities during one full PWM period does not hold any more.

The project goal – sensor fault detection with all-digital self-sensing - within the active magnetic bearing system with supreme reliability is fulfilled even with the low available number of samples per PWM period and the simple algorithm for air gap calculation.

For the application of this self-sensing concept for sensor replacement, higher sampling rates and sophisticated algorithms for air gap calculation, especially for small air gaps, have to be used.

#### ACKNOWLEDGMENT

The authors gratefully acknowledge the support of this project by the Austrian Science Fund “Fonds zur Förderung der wissenschaftlichen Forschung (FWF)” and by the city of Vienna “Hochschuljubiläumsstiftung der Stadt Wien”.

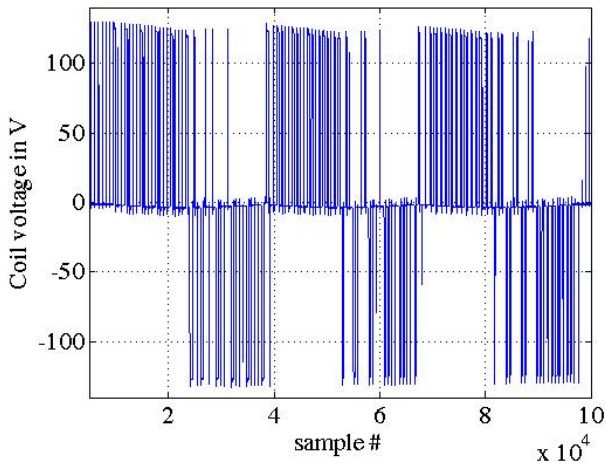


Fig. 7 Electro magnet coil voltage of one complete test cycle for  $s_{g\_REF} = 0.5$  mm

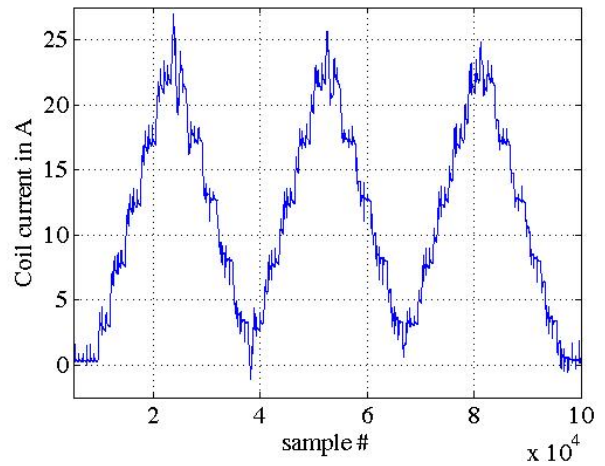


Fig. 10 Electro magnet coil current of one complete test cycle for  $s_{g\_REF} = 0.5$  mm

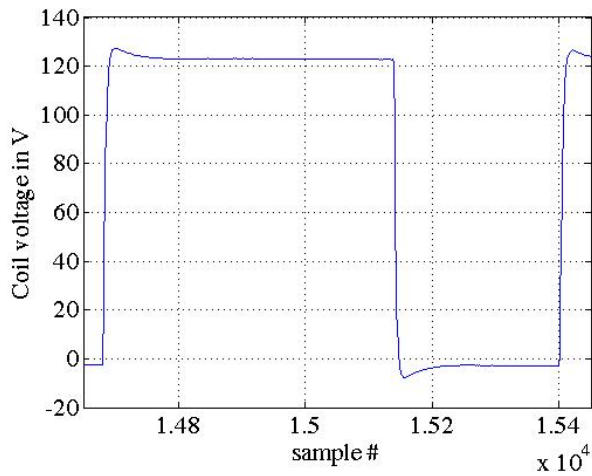


Fig. 8 Electro magnet coil voltage of one PWM period with positive amplifier output voltage (pulse width = 66%) for  $s_{g\_REF} = 0.5$  mm

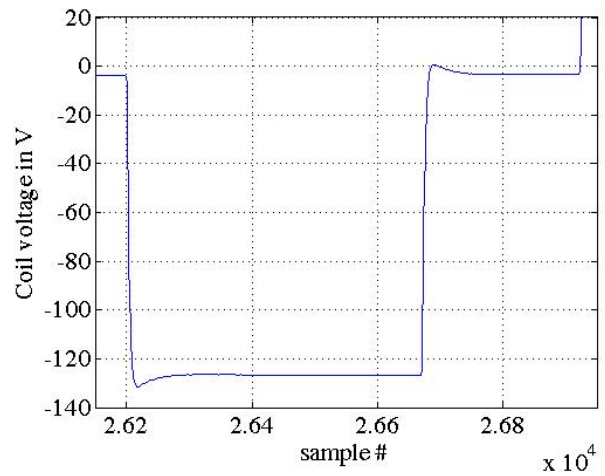


Fig. 11 Electro magnet coil voltage of one PWM period with negative amplifier output voltage (pulse width = 66%) for  $s_{g\_REF} = 0.5$  mm

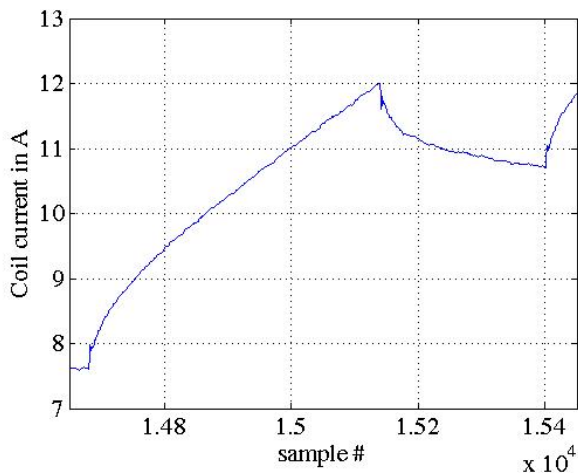


Fig. 9 Electro magnet coil current of one PWM period with positive amplifier output voltage (pulse width = 66%) for  $s_{g\_REF} = 0.5$  mm

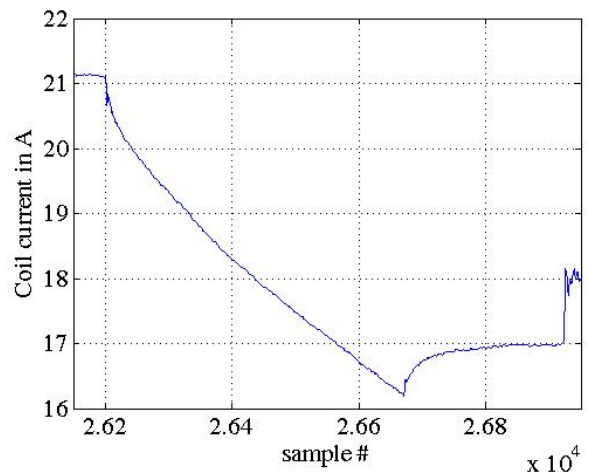


Fig. 12 Electro magnet coil current of one PWM period with negative amplifier output voltage (pulse width = 66%) for  $s_{g\_REF} = 0.5$  mm

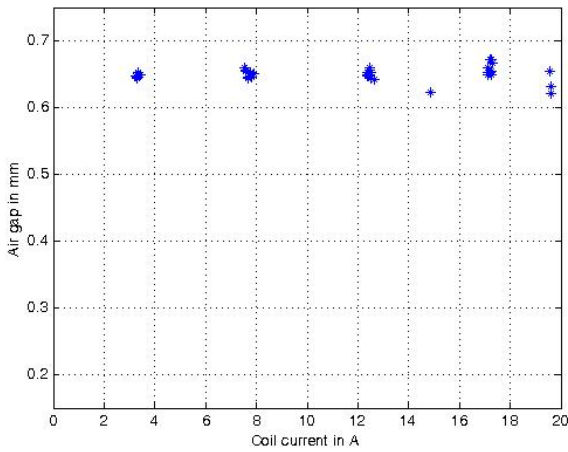


Fig. 13 Self-sensing result for  $s_{g\_REF} = 0.65$  mm against coil current (pulse width = 45 % - 67 %)

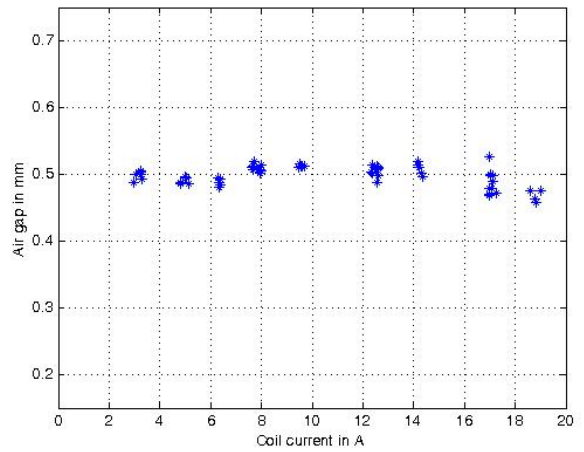


Fig. 16 Self-sensing result for  $s_{g\_REF} = 0.5$  mm against coil current (pulse width = 45 % - 67 %)

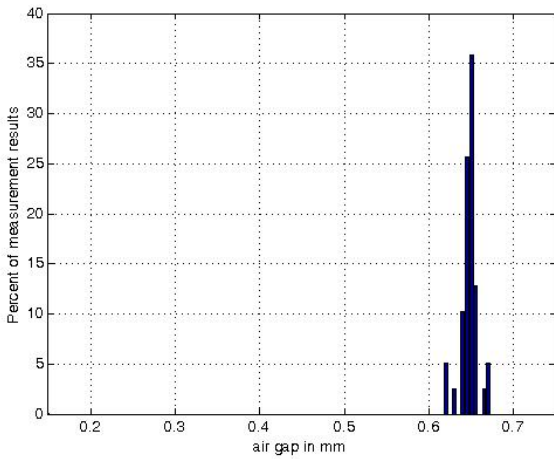


Fig. 14 Histogram for  $s_{g\_REF} = 0.65$  mm (pulse width = 45 % - 67 %)

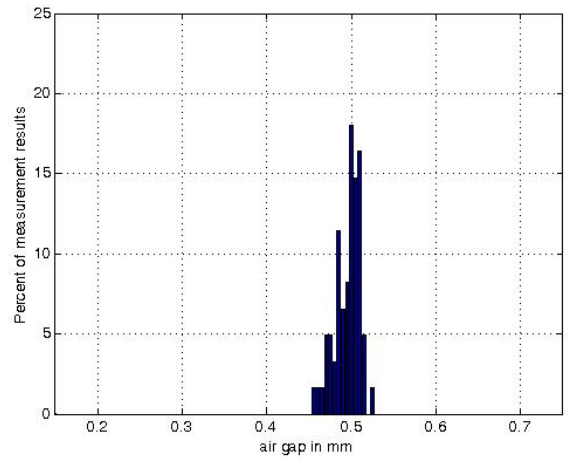


Fig. 17 Histogram for  $s_{g\_REF} = 0.5$  mm (pulse width = 45 % - 67 %)

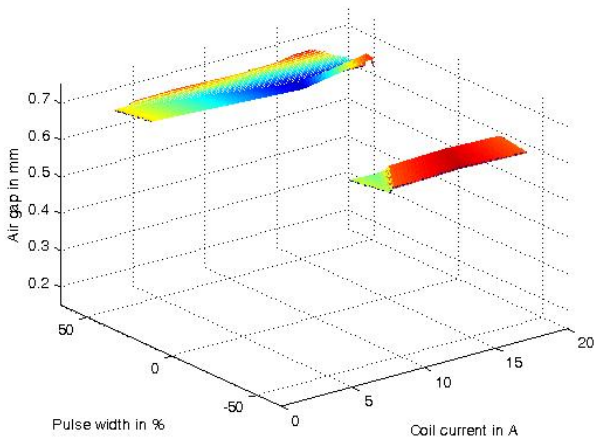


Fig. 15 Self-sensing result for  $s_{g\_REF} = 0.65$  mm against coil current and pulse width (here, negative pulse widths stand for negative amplifier output voltages with the corresponding pulse width)

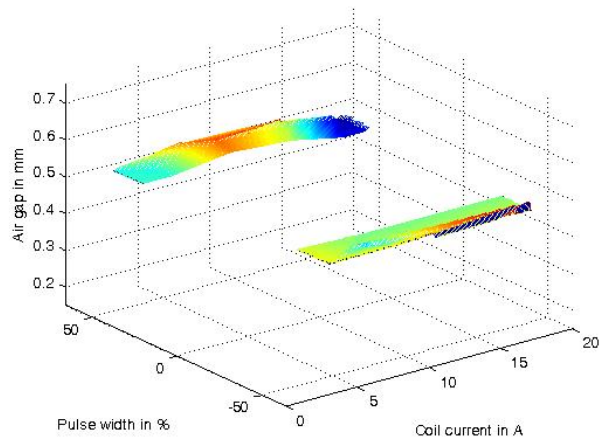


Fig. 18 Self-sensing result for  $s_{g\_REF} = 0.5$  mm against coil current and pulse width (here, negative pulse widths stand for negative amplifier output voltages with the corresponding pulse width)

## REFERENCES

- [1] R. Gurumoorthy, W. L. Soong, J. P. Lyons, and A. F. Storace. Implementation of sensorless control of radial magnetic bearings. in Proc. *MAG '95 - Magnetic Bearings, Magnetic Drives and Dry Gas Seals Conference & Exhibition*, pages 239–248, Alexandria, Virginia, August 10-11 1995.
- [2] B. V. Jayawant, B. E. Dawson, R. J. Whorlow, and J. C. Peyton Jones. Digitally controlled transducerless magnetic suspension system. in *IEE Proceedings of Science, Measurement and Technology*, volume 143, pages 47 – 51, January 1996.
- [3] L. Kucera. Robustness of self-sensing magnetic bearing. in Proc. *Magnetic Bearings Industrial Conf.*, pages 261 – 270, Alexandria, VA, 1997.
- [4] Lichuan Li, T. Shinshi, and A. Shimokohbe. State feedback control for active magnetic bearings based on current change rate alone. *IEEE Transactions on Magnetics*, 40(6):3512 – 3517, November 2004.
- [5] D. Montie. *Performance Limitations and Self-Sensing Magnetic Bearings*. PhD-thesis, University of Virginia. January 2003.
- [6] M.D. Noh and E.H. Maslen. Self-sensing magnetic bearings using parameter estimation. *IEEE Transactions on Instrumentation and Measurement*, 46(1):45 – 50, February 1997.
- [7] Y. Okada, K. Matsuda, and B. Nagai. Sensorless magnetic levitation control by measuring the PWM carrier frequency component. in Proc. *3rd Int. Symp. on Magnetic Bearings*, pages 176–183, Alexandria, Virginia, July 29-31 1992.
- [8] A. Schammas, R. Herzog, P. Buehler, and H. Bleuler. New results for self-sensing active magnetic bearings using modulation approach. *IEEE Transactions on Control Systems Technology*, 13(4):509 – 516, July 2005.
- [9] A. Schulz, M. Neumann, J. Wassermann, A Sophisticated Active Magnetic Bearing System with Supreme Reliability, in Proc. *11th Int. Symp. on Magnetic Bearings*, Nara, Japan, Aug. 26-29 2008.
- [10] A. Schulz, A. Gamez Sangra M. Neumann, J. Wassermann, Modelling and simulation of a sophisticated active magnetic bearing system, in Proc. *X. Int. Conf. Theory of Machines and Mechanisms, IFToMM*, Liberec, Czech Repub., Sep. 2-4 2008
- [11] A. Schulz, M. Neumann, J. Wassermann, A Sophisticated Concept for Supreme AMB Reliability, in Proc. *9th International Conference on Motion and Vibration Control - Movic 2008*, Munich, Germany, Sep. 15-18 2008.
- [12] A. Schulz, M. Neumann, J. Wassermann, Modeling and Simulation of a Hot-Swap Controller Amplifier Module for an Active Magnetic Bearing with Supreme Reliability, in Proc. *9th International Conference on Modeling and Simulation of Electric Machines, Converters and Systems - Electrimacs 2008*, Quebec, Can., Jun. 8-11.
- [13] A. Schulz, Simulation eines ausfallsicheren aktiven Magnetlagers, in Proc. *Schwingungen in rotierenden Maschinen - SIRM 2009*, Vienna, Austria, February 23-25 2009.
- [14] A. Schulz, A hot-swap controller amplifier module for active magnetic bearings with supreme reliability - electronic circuitry and error detection strategies, in Proc. *20th International Symposium on Power Electronics, Electrical Drives, Automation and Motion - Speedam 2010*, Pisa, Italy, June 14-16 2010.
- [15] A. Schulz, An All-Digital Self-Sensing Concept, *IEEE Transactions on Magnetics*, (not published - in preparation)
- [16] G. Schweizer, E.H. Maslen, *Magnetic Bearings: Theory, Design, and Application to Rotating Machinery*, Berlin Heidelberg: Springer-Verlag, 2009.
- [17] P. Tsao, S.R. Sanders, and G. Risk. A self-sensing homopolar magnetic bearing: analysis and experimental results. in Proc. *Industry Applications Conference*, volume 4, pages 2560 – 2565, October 3 - 7 1999.
- [18] D. Vischer. *Sensorlose und spannungsgesteuerte Magnetlager*. PhD thesis, Eidgenössische Technische Hochschule (ETH) Zurich, Switzerland, 1988.